Cerebral Cortex, October 2021;31: 4595–4611

https://doi.org/10.1093/cercor/bhab108
Advance Access Publication Date: 3 May 2021
Original Article

ORIGINAL ARTICLE

Claustral Input to the Macaque Medial Posterior Parietal Cortex (Superior Parietal Lobule and Adjacent Areas)

Michela Gamberini[1], Lauretta Passarelli[1], Daniele Impieri[1], Giulia Montanari[1], Stefano Diomedi[1], Katrina H. Worthy[2,3], Kathleen J. Burman[2], David H. Reser[2,4], Patrizia Fattori[1], Claudio Galletti[1], Sophia Bakola[2,3,†] and Marcello G. P. Rosa[2,3,†]

[1]Department of Biomedical and Neuromotor Sciences, University of Bologna, 40126 Bologna, Italy, [2]Department of Physiology and Neuroscience Program, Biomedicine Discovery Institute, Monash University, Clayton, Victoria 3800, Australia, [3]Australian Research Council, Centre of Excellence for Integrative Brain Function, Monash University Node, Clayton, Victoria 3800, Australia and [4]Graduate Entry Medicine Program, Monash Rural Health-Churchill, Churchill, Victoria 3842, Australia

Address correspondence to Sophia Bakola. Email: sofia.bakola@monash.edu; Marcello G. P. Rosa. Email: marcello.rosa@monash.edu
[†]Joint corresponding authors.

Abstract

The projections from the claustrum to cortical areas within and adjacent to the superior parietal lobule were studied in 10 macaque monkeys, using retrograde tracers, computerized reconstructions, and quantitative methods. In contrast with the classical view that posterior parietal areas receive afferents primarily from the dorsal and posterior regions of the claustrum, we found that these areas receive more extensive projections, including substantial afferents from the anterior and ventral regions of the claustrum. Moreover, our findings uncover a previously unsuspected variability in the precise regions of the claustrum that originate the projections, according to the target areas. For example, areas dominated by somatosensory inputs for control of body movements tend to receive most afferents from the dorsal-posterior claustrum, whereas those which also receive significant visual inputs tend to receive more afferents from the ventral claustrum. In addition, different areas within these broadly defined groups differ in terms of quantitative emphasis in the origin of projections. Overall, these results argue against a simple model whereby adjacency in the cortex determines adjacency in the sectors of claustral origin of projections and indicate that subnetworks defined by commonality of function may be an important factor in defining claustrocortical topography.

Key words: claustrum, connectivity, primate, sensorimotor integration, superior parietal lobule

Introduction

The claustrum is a thin layer of gray matter interposed between the insular cortex and the striatum. In primates, the claustrum has widespread connections with the cortex, which follow a coarse topographic organization (Pearson et al. 1982; Baizer et al. 1993; Edelstein and Denaro 2004; Baizer et al. 2014; Gattass et al. 2014; Mathur 2014; Reser et al. 2014; Smythies et al. 2014; Milardi et al. 2015; Torgerson et al. 2015; Brown et al. 2017; Gamberini et al. 2017; Reser et al. 2017). This extensive connectivity has generated various hypotheses of claustrum function, including the integration of sensorimotor inputs (an important element of conscious experiences; Crick and Koch 2005) and the synchronization of cognitive processes across cortical networks

(Smythies et al. 2012a, 2012b, 2014; Gattass et al. 2014; Mathur 2014; Reser et al. 2014; Torgerson et al. 2015; Brown et al. 2017). Recently, hypotheses regarding claustrum function have converged on three main themes: modulation of salience processing and behavioral choice (especially under conditions of high cognitive demand; Patru and Reser 2015; Smith, Watson, et al. 2019; White et al. 2020); modulation of various attention dependent processes (Goll et al. 2015; Atlan et al. 2018; Jackson 2018); and modulation or synchronization of cortical oscillatory activity, especially slow wave activity (Narikiyo et al. 2020). However, the functions of the claustrum remain undetermined.

The recent emphasis on salience and attention processing results in part from elegant and detailed studies of claustrum connections to anterior areas of the cortex, especially anterior cingulate and prefrontal regions. In contrast, knowledge about the claustrum projections to posterior cortical areas has not been equally emphasized in modern studies. Here, we report on the claustral input to areas of the macaque superior parietal lobule (SPL) and adjacent cortex in the intraparietal sulcus and midline. Different SPL areas are involved in processing and integration of information coming from different sensory modalities, in many cases contributing to the control of reaching and grasping actions (Kalaska 1996; Andersen and Cui 2009; Fattori et al. 2012, 2017; Mai and Paxinos 2012; Galletti and Fattori 2018). According to classical cytoarchitecture (Brodmann 1909), the primate SPL includes part of cytoarchitectural area 7, posteriorly, and area 5 anteriorly. In the macaque, a recent review by Gamberini et al. (2020) proposed that the SPL part of cytoarchitectural area 7 includes at least four functionally defined areas (PEc, V6A, PGm, and MIP), which are bounded both laterally and medially by other subdivisions of area 7 (e.g., areas LIP and PGm; Fig. 1A). Likewise, area 5 includes at least three functional subdivisions (PE, PEci, and PEip) and is bounded medially by cortex which shares emphasis on sensorimotor function (e.g., area 31; Fig. 1A). Our laboratories have previously described the claustral input to areas PE, PEc and the adjoining somatosensory area 2 (Gamberini et al. 2017). Here, we contrast those findings with new observations following retrograde tracer injections in a number of posterior parietal areas centered on the SPL, including the intraparietal sulcus and the mesial surface of the hemisphere. The present results provide the most comprehensive survey to date of the claustral input to the macaque posterior parietal cortex and provide evidence supporting a model whereby functional similarity, not physical adjacency is the organizing principle underlying the pattern of claustrocortical projections.

Materials and Methods

Injections of retrograde neuronal tracers were performed in the medial posterior parietal cortex of 10 macaque monkeys (7 *Macaca fascicularis*, 2 *Macaca nemestrina*, and 1 *Macaca mulatta*). The location and extent of the injection sites are summarized in Table 1 and Figure 1. Experimental protocols followed the Australian Code of Practice for the Care and Use of Animals for Scientific Purposes, the European Union Directive 86/609/EEC, and the revised Directive 2010/63/EU. The Monash University Animal Experimentation Ethics Committee and the University of Bologna Bioethics Committee approved the experimental procedures (University of Bologna Permit N° 170/2015-PR, 19/03/2015; Monash University Permits N° MARP2012/082, SOBSA/P/2010/05, SOBSA/P/2010/28).

Surgical Procedure

The experimental procedures followed those detailed in previous publications (Bakola et al. 2017; Gamberini et al. 2017; Passarelli et al. 2018). Surgeries were performed under aseptic conditions, and in all cases heart rate, respiratory cycle, blood pressure, and body temperature were monitored. The protocol for induction and maintenance of anesthesia varied given the procedures approved by the two Universities as well as refinements introduced during the project. Details of the drugs administered to each animal are summarized in Table 2. Hydration in these cases was provided by constant i.v. infusion of Hartmann's solution. Dexamethasone (0.3 mg/kg, i.m.) and Norocillin (25 mg/kg, i.m.) were also administered at the beginning of the procedures.

The animals were placed in a stereotaxic frame, and a craniotomy was performed over the posterior parietal cortex. In some cases (9–15; see Table 1), in order to reach the mesial surface of the hemisphere, a portion of the posterior parietal cortex of the contralateral hemisphere was retracted or removed by aspiration, and the mesial surface exposed by creating a window in the falx cerebri. Injection sites were selected by visual inspection using several sulci (the cingulate, parieto-occipital, and intraparietal sulci) and blood vessels as landmarks, and were later assigned to architectonic subdivisions after histological examination of postmortem material.

Fluorescent retrograde neuronal tracers (Fast Blue, FB; Diamidino Yellow, DY; Cholera toxin B subunit conjugated with Alexa fluor 488, CTBgreen; Fluoro Ruby, FR) were injected using microsyringes fitted with glass micropipettes at the tips of the needles. In cases 9 and 11, crystals of fluorescent tracers (FB and DY, each crystal 100–200 µm in diameter) were directly inserted into the cortex, after being captured by electrostatic attraction at the tip of tungsten rods (Rosa et al. 2005). In all cases, after injections, the cortical surface was covered with Gelfilm®, the bone flap was fixed back in place with dental acrylic, and muscles and skin were sutured. Upon recovery from anesthesia, the animals were monitored by veterinary staff. For the following 2–3 days, they received analgesics and antibiotics (Table 2).

Tissue Processing

After a survival time of 14 days, the animals were anesthetized as above, before receiving a lethal dose i.v. of sodium thiopental or pentobarbital (100 mg/kg) injection. They were perfused with heparinized saline or phosphate buffer, and then with 4% paraformaldehyde in 0.1 M phosphate buffer at pH 7.4. Cases ANA9 and ANA10 were subsequently perfused with 4 L of 5% glycerol in the same buffer. The brains were removed from the skull, photographed, and then immersed for cryoprotection in fixative solutions containing sucrose (10–30%; most animals) or glycerol (10–20%; animals ANA9 and ANA10) until they sank. Following rapid freezing of the tissue blocks with isopentane or dry ice, coronal sections (50 µm in most cases and 60 µm in ANA9 and ANA10) were obtained. One in five sections was left unstained for observation under a fluorescence microscope. Adjacent sections were stained for Nissl substance, myelin, and cytochrome oxidase (for detailed histological protocols, see http://www.marmosetbrain.org/reference).

Data Analysis

The unstained sections were scanned for labeled neurons under fluorescence illumination (for details, see Gamberini et al.

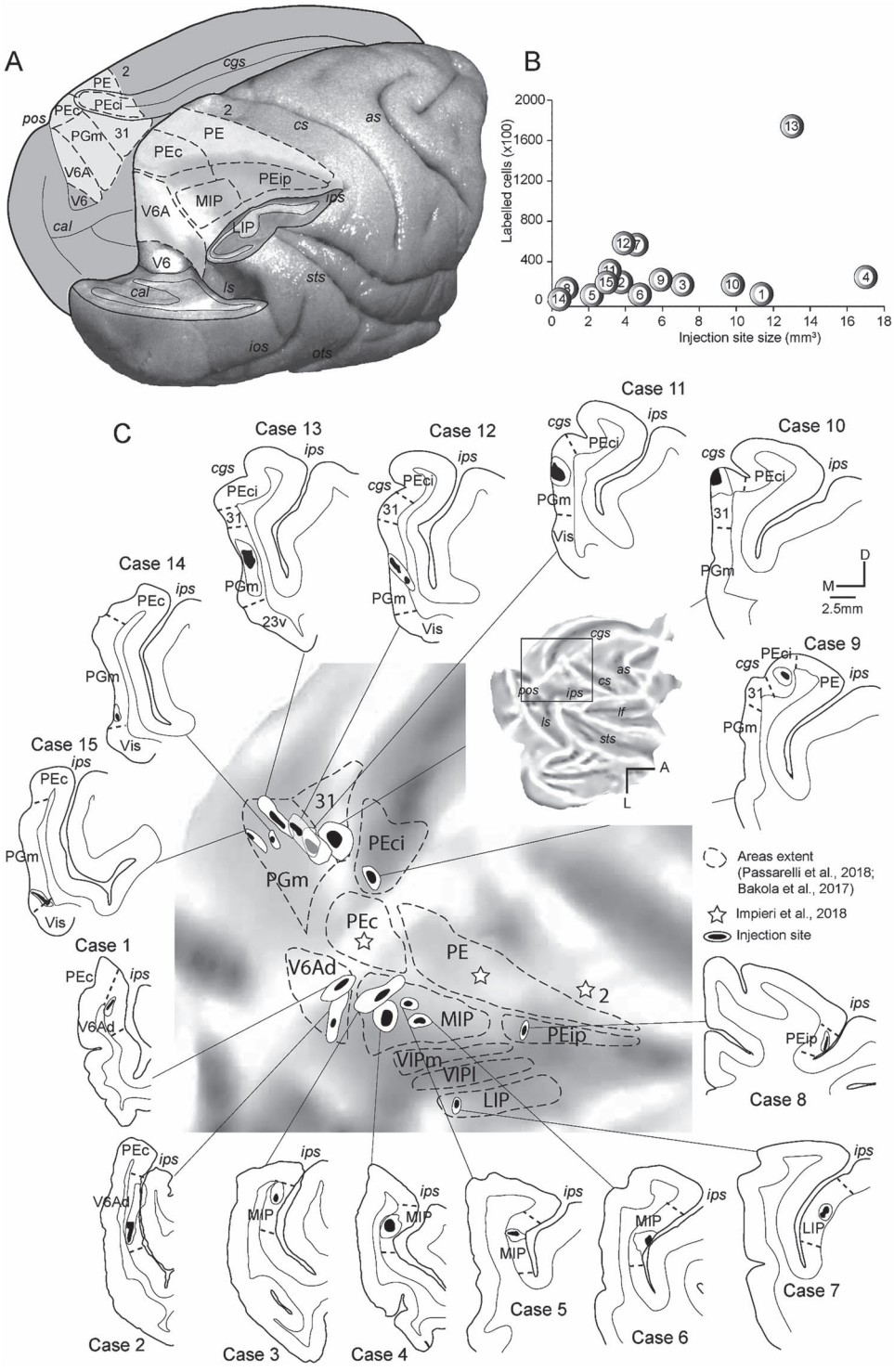

Figure 1. Summary of injection site locations. (*A*) Posterolateral view of macaque brain. The right hemisphere has been partially dissected at the level of the fundus of intraparietal, parietooccipital, and lunate sulci to show the hidden cortex of SPL. The medial surface of the left hemisphere is also visible, with the cingulate sulcus open to show area PEci. Dashed lines delimit different cortical areas of SPL. (*B*) Scatter plot showing the size of the injection site (in mm^3) in relation to the number of labeled cells in the entire hemisphere. (*C*) Summary of locations of injection sites. Coronal sections showing the centers (black) and halos (white) of injection sites for each of the cases presented in this study. The boundaries of areas are also shown. A summary of the injection sites for V6Ad (cases 1 and 2), MIP (cases 3-6), LIP (case 7), PEip (case 8), PEci (case 9), area 31 (case 10), and PGm (11-15) is presented on the unfolded reconstruction of a macaque left hemisphere (expanded view in the top right). The dashed lines indicate the approximate extent of areas according to previous studies (Bakola et al. 2017; Passarelli et al. 2018). White symbols indicate the approximate locations of injection sites in neighboring areas according to a previous study (Impieri et al. 2018). Abbreviations: cal, calcarine sulcus; cgs, cingulate sulcus; ips, intraparietal sulcus; pos, parieto-occipital sulcus; ls, lunate sulcus; cs, central sulcus; lf, lateral fissure; as, arcuate sulcus; sts, superior temporal sulcus; V6, V6A, MIP, LIP, VIP, PEc, PE, PEip, S1, PGm, 31, PEci are designations of cortical areas; D, dorsal; M, medial; L, lateral; A, anterior.

Table 1

Case[1]	Denomination	Species	Injected area	Tracer	Amount and concentration	Claustral cells	Total labeled neurons
1[a]	MF7	*M. fascicularis*	V6A	DY[2]	0.3 microl, 1.5% in PB	49	7340
2	NF228	*M. nemestrina*	V6A	DY[2]	0.25 microl, 1.5% in PB	312	19 653
3	NM31	*M. nemestrina*	MIP	FB[3]	0.35 microl, 1.5% in DW	1680	17 265
4[a]	MF7	*M. fascicularis*	MIP	FB[3]	0.3 microl, 1.5% in DW	883	23 294
5	ANA10	*M. mulatta*	MIP	CTBgreen[4]	2 microl, 1% in PBS	311	6125
6[b]	ANA9	*M. fascicularis*	MIP	CTBgreen[4]	2 microl, 1% in PBS	213	7238
7	MF8	*M. fascicularis*	LIP	DY[2]	0.3 microl, 1.5% in PB	536	55 464
8	MF10	*M. fascicularis*	PEip	DY[2]	0.25 microl, 1.5% in PB	91	6704
9[b]	ANA9	*M. fascicularis*	PEci	DY[2]	1 crystal	879	21 214
10[b]	ANA9	*M. fascicularis*	31	FB[3]	0.2 microl, 1% in DW	1086	16 999
11	MF3	*M. fascicularis*	PGm	FB[3]	1 crystal	1108	27 096
12[c]	MF6	*M. fascicularis*	PGm	FB[3]	0.35 microl, 1.5% in DW	2896	58 036
13[d]	MF4	*M. fascicularis*	PGm	DY[2]	1 microl, 1% in PB	4334	174 222
14[d]	MF4	*M. fascicularis*	PGm	FR[4]	0.4 microl, 10% in saline	53	2641
15[c]	MF6	*M. fascicularis*	PGm	DY[2]	0.35 microl, 1.5% in PB	730	20 554

[1]The letters a, b, c and d indicate injections placed in the same hemisphere.
[2]Sigma Aldrich.
[3]Polysciences Europe, Germany.
[4]Molecular Probes.
Abbreviations: DY, Diamidino Yellow; FB, Fast Blue; CTB, cholera toxin B; FR, Fluoro-Ruby; PB, phosphate buffer; DW, distilled water PBS, phosphate-buffered saline.

Table 2

Animal	Premedication drug: dose, administration route	Anesthesia (induction) drug: dose, administration route	Anesthesia (maintenance) drug: dose, administration route	Postoperative analgesia drug: dose, administration route
ANA9	atropine: 0.04 mg/kg, i.m. ketamine hydrochloride: 15 mg/kg, i.m.	sodium thiopental: 8 mg/kg, i.v.	sodium thiopental: 8 mg/kg, i.v. (when necessary)	Ketorolac: 1 mg/kg, i.m. Erythromycin: 1–1.5 mL/10 kg i.m. Norocillin: 0.1–0.2 mL/kg i.m.
ANA10	atropine: 0.04 mg/kg, i.m. dexmedetomidine hydrochloride: 2.5 µg/kg, i.m. ketamine hydrochloride: 15 mg/kg, i.m.	dexmedetomidine hydrochloride (solution in saline): 1.65 µg/kg/L; flow rate 70–60 mL/h, i.v.	sodium thiopental: 8 mg/kg, i.v. (when necessary)	Ketorolac: 1 mg/kg, i.m. Erythromycin: 1–1.5 mL/10 kg i.m.
MF3 MF4	diazepam: 3.0 mg/kg, i.m. atropine: 0.2 mg/kg, i.m.	alfaxalone: 10 mg/kg, i.m.	alfaxalone: 5 mg/kg, i.v. (when necessary)	Ketorolac: 1 mg/kg, i.m. Carprofen: 5 mg/kg, s.c. Erythromycin: 1–1.5 mL/10 kg i.m. Norocillin: 0.1–0.2 mL/kg i.m.
MF6 NM31 MF7 MF8 MF10 NF228	diazepam: 1.0 mg/kg, i.m. atropine: 0.04 mg/kg, i.m.	ketamine-medetomidine-butorphanol: 0.1 mg/kg, i.m.	isoflurane (animal intubated): 0.5–2%	Temgesic: 0.01 mg/kg, i.m. Carprofen: 4 mg/kg, s.c. Erythromycin: 1–1.5 mL/10 kg i.m. Norocillin: 0.17 mL/kg i.m.

2017; Bakola et al. 2017; Passarelli et al. 2018). In each case, the entire hemisphere ipsilateral to the injection site was examined for retrograde label. For all sections examined, the outer and inner boundaries of the cerebral cortex, the outlines of the injection sites, and the location of labeled cells were mapped at 500–600 µm intervals (1 in 10 sections) using a digitizing system attached to the microscopes (MD3 digitizer and MDPlot software, Accustage). The histological criteria used for the definition of the boundaries of areas around the injection sites have been fully described in previous publications (Pandya and Seltzer 1982; Morecraft et al. 2004; Luppino et al. 2005; Passarelli et al. 2011, 2018; Bakola et al. 2017). The present report focuses on injections confined in single architectonic areas, although data from injections that crossed areal boundaries have been used as comparison and confirmation of particular aspects of the data, as detailed in Results.

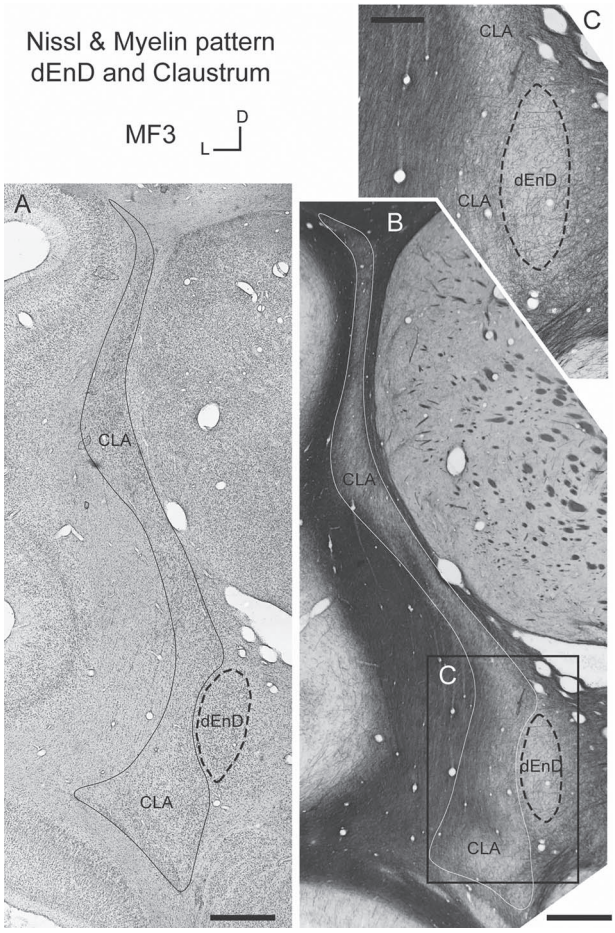

Figure 2. Architecture of insular Claustrum (CLA) and dorsal Endopiriform nucleus (dEnD). (*A*, *B*) Low-power photomicrographs showing the cytoarchitectural (*A*) and myeloarchitectural (*B*) patterns of CLA and dEnD in representative coronal sections from animal MF3. Scale bar = 1 mm. (*C*) Higher power photomicrograph of the representative ventral portion of the claustrum where dEnD becomes evident, taken at the level indicated on the inset in *B*. Scale bar = 500 µm.

The limits of the claustrum were outlined using sections stained with the Nissl method. The limit between the insular claustrum and the dorsal endopiriform nucleus was defined using the neighboring sections stained with the Gallyas method (Miyashita et al. 2005; Pham et al. 2019; Smith, Alloway, et al. 2019). A representative example is shown in Figure 2. For the present paper, both subdivisions were considered as a single structure, with the location of the endopiriform nucleus indicated in the illustrations. Three-dimensional reconstructions of this complex were obtained using the CARET software package (Van Essen et al. 2001). As previously described (Galletti et al. 2005; Gamberini et al. 2009), mid-thickness contours of cortical gray matter were used to align brain sections in order to reconstruct the brain surface in each case. Adjustments were applied to claustral contours to improve local alignment, when necessary.

Density maps obtained from the coordinates of single labeled cells were superimposed on the 3D reconstructions. The representation of the density maps was computed with the software R (Team 2014) using the package ggplot2 (Wickham 2009). The region of the claustrum containing the highest number of labeled neurons was considered as reference, and the density of neurons was expressed as a percentage of this maximum value (Rosa et al. 2009).

For regional analysis of the location of labeled cells, we followed a subdivision similar to that proposed by Pearson et al. (1982). As a first step, the centroid of the reconstructed claustrum was calculated using the measure function in ImageJ (FIJI; v.1.47n; NIH, USA), applied to an outline of the 3D claustrum reconstruction from CARET. On the basis of the centroid, the shape of the reconstructed claustrum was then subdivided into four quadrants of equal size, and the analysis of the location of labeled neurons was then performed with reference to anterior-dorsal (A-D), anterior-ventral (A-V), posterior-dorsal (P-D), and posterior-ventral (P-V) quadrants (Gamberini et al. 2017).

In order to standardize the cases, we also performed a second type of analysis, based on the subdivision of the claustrum into equal intervals along its anteroposterior extent, defined by coronal sections. Specifically, the distribution of retrograde labeling in the claustrum was analyzed in 10 intervals, each interval corresponding to 10% of the extent of the claustrum along the anteroposterior axis. In order to compare cases, we performed a piecewise polynomial interpolation using cubic Hermite polynomial (Matlab function "pchip") on the distribution of retrograde labeled cells. In order to evaluate the similarity in the distribution of labeled cells across different injections, we employed the Kendall rank correlation coefficient W (Siegel 1956; Legendre 2005), which measures the agreement between sets of ranks. Kendall coefficient W values vary from 0 in the case of complete disagreement to 1 in the case of perfect agreement. The statistical significance of these measures was computed with adjusted χ^2 (Friedman's χ^2). We first tested the similarity between injections within the same area. If the distributions resulted statistically equal (adjusted χ^2, $P < 0.05$), we summed the cell counts of the relevant cases, obtaining a unique distribution assigned to that area. Finally, we compared the similarity across areas (using both interval and quadrant distribution).

Results

We report on the results of 15 tracer injections (Table 1 and Fig. 1). The main focus will be on areas PGm and MIP, which received 5 and 4 injections, respectively, allowing the estimation of the degree of variability within each area. Results from these injections will then be compared with new data on the claustral projections to nearby areas V6Ad (2 injections), 31, PEci, PEip, and LIP (1 injection each). Together with our previous observations regarding areas PE and PEc (Gamberini et al. 2017), this provides the first comprehensive view of the claustral afferents to medial posterior parietal areas. Examples of sections through the injection sites and of aggregations of labeled neurons in the claustrum are illustrated in Supplementary Figure 1.

The numbers of labeled neurons in the claustrum formed a small proportion of the total label revealed by the injections. As shown in Table 1, claustral afferents corresponded on average to 3.59% (s.d. = 2.37) of the total number of labeled neurons in a hemisphere.

Area PGm

Five injections were confined within area PGm, on the mesial surface of the hemisphere (cases 11–15). In a previous report,

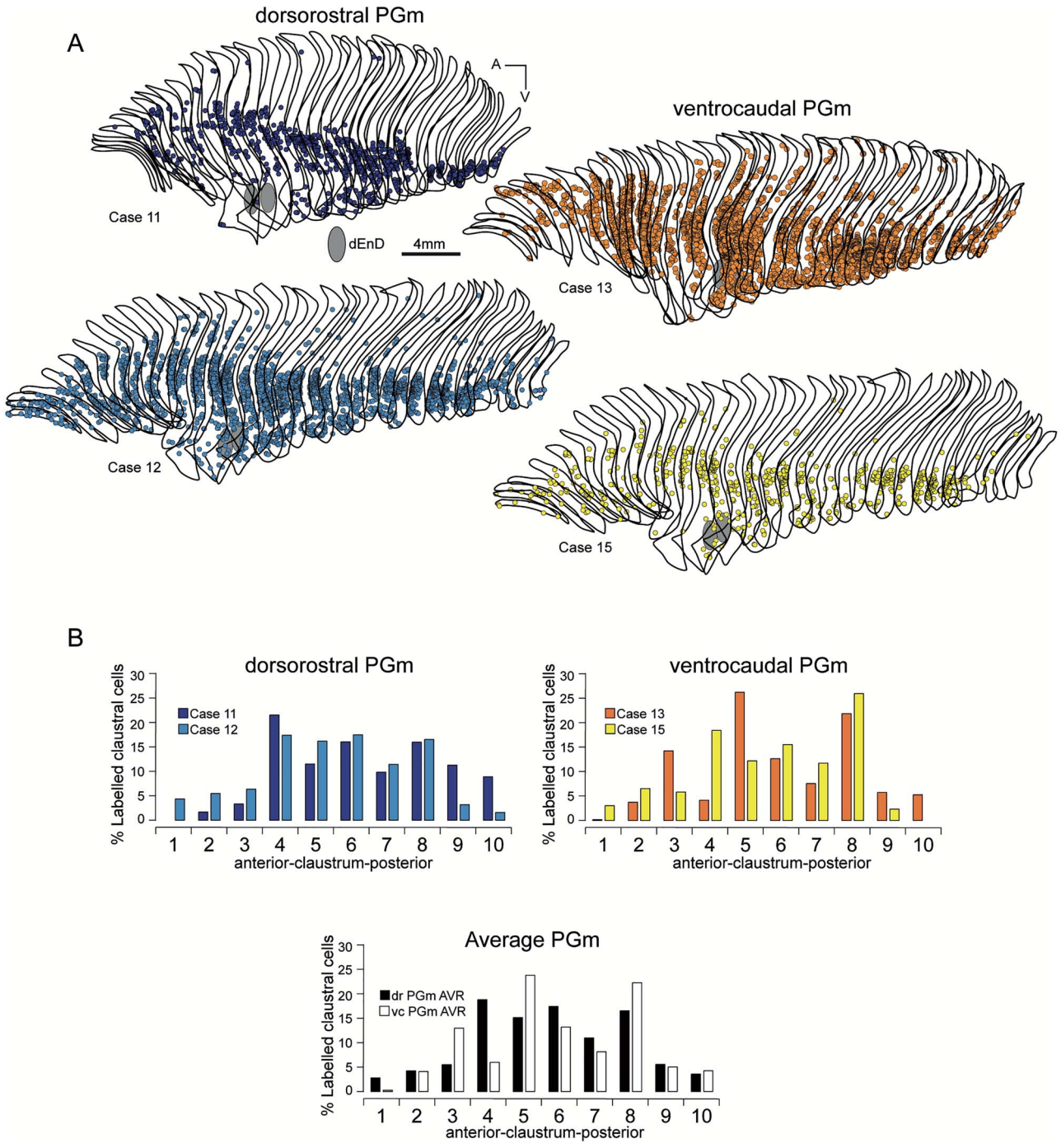

Figure 3. Claustral afferents to dorsorostral and ventrocaudal sectors of area PGm. (A) Outlines of the claustrum, sectioned in the coronal plane. Locations of single labeled neurons are shown as colored circles; gray region represents the location of dEnD. In this and other figures, the claustrum is represented with the anterior end at the left, irrespective of the hemisphere injected, to facilitate comparisons. Scale bar = 4 mm. (B) Percentage of labeled cells in intervals each representing 10% of the claustrum extent along the rostro-caudal axis. Abbreviations: A, anterior; P, posterior. Other details and abbreviations as in Figure 1.

we have described connectional differences between the dorsorostral and ventrocaudal sectors of this area, with the latter showing relatively denser afferents from visual cortical areas (Passarelli et al. 2018). Here, two of the cases (11 and 12) had injections in dorsorostral PGm, and three (13–15) in the ventrocaudal PGm.

Digital reconstructions of the claustrum in four cases are illustrated in Figure 3A. These reconstructions show that labeled cells were distributed across the entire rostrocaudal extent of the claustrum, forming a continuous stripe of variable width on the ventral part of this structure (but sparser in its ventral region, near the temporal pole). For quantification, we subdivided the

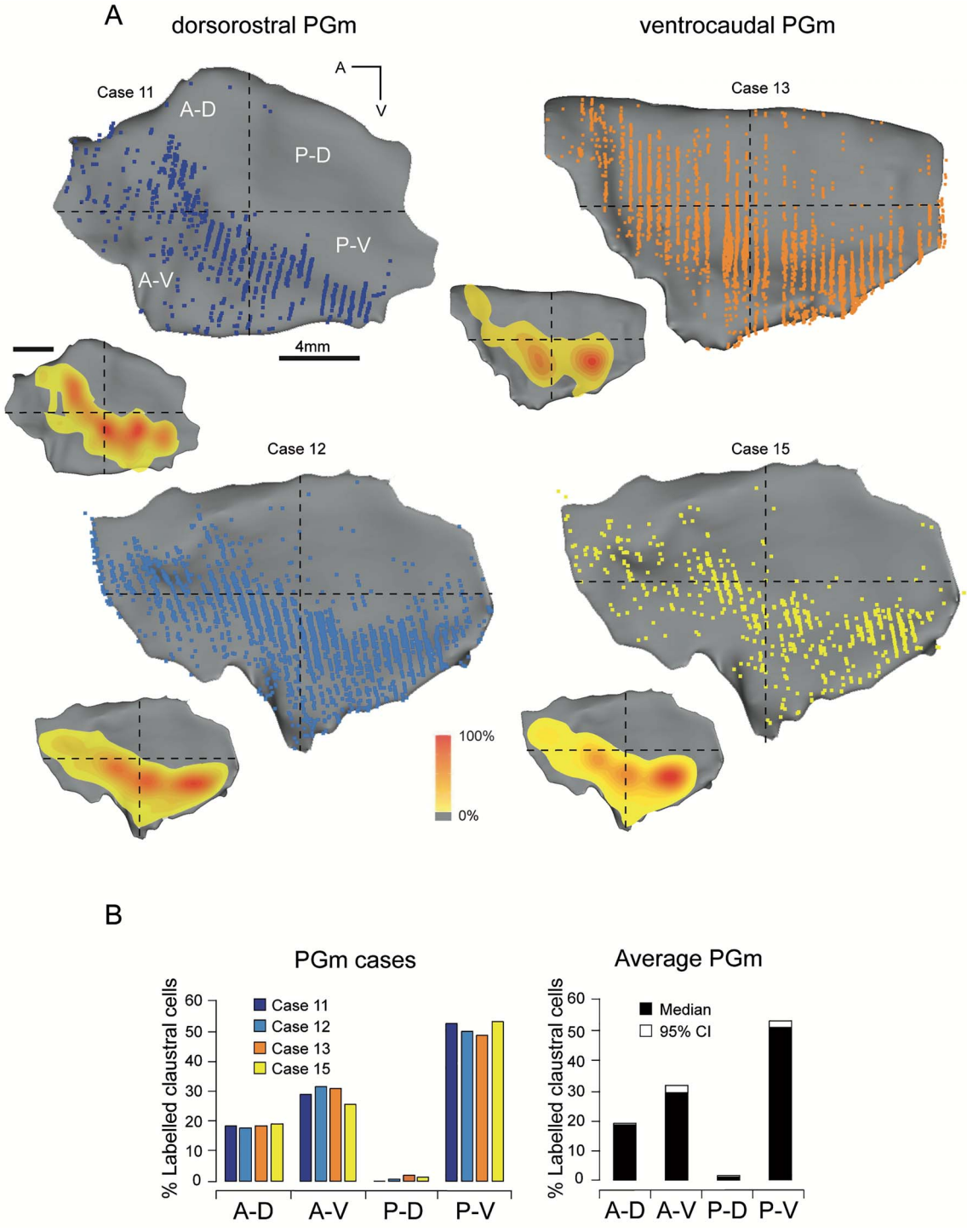

Figure 4. Claustral afferents to area PGm. (*A*) Medial views of 3D reconstructions of the claustrum in the PGm injection cases shown in Figure 3, illustrating the distribution (single colored dots) and density (in color scale) of labeled cells. Color scale indicates the relative density of labeled cells, counted within 300 × 300 µm units, as a percentage of the maximum value. Scale bar = 4 mm. (*B*) Percentage of labeled cells in the four quadrants of the claustrum after injections confined within the myeloarchitectonic limits of area PGm (Passarelli et al. 2018). On the right, the averaged values represent the medians (in black) and the 95% confidence interval (in white). Other details and abbreviations as in Figures 1 and 3.

claustrum of each case in 10 anteroposterior intervals. The results of this analysis (Fig. 3B) show that cases with injections in the dorsorostral and in ventrocaudal part of PGm have a similar distribution. Case 14 (not shown) had relatively few labeled neurons, likely because of a smaller injection site; nonetheless, the distribution was very similar to that found in the four illustrated cases.

Figure 4A shows 3D volumetric reconstructions of the claustrum of the same cases. Figure 4B indicates the fraction of labeled cells in each quadrant for each of the four cases (Fig. 4B,

left), and as an average in the quadrants of all cases (Fig. 4B, right). In the anterior half of the claustrum, labeled cells were present both dorsally and ventrally, though being slightly more abundant ventrally (30% ± 2.4% in the anterior-ventral [A-V] sector; 18% ± 0.5% in the anterior-dorsal [A-D] sector). In the posterior half of the claustrum, labeled cells were concentrated in the posterior-ventral quadrant (P-V; 52% ± 2.1%), with only a few cells located in the posterior-dorsal (P-D) quadrant (1% ± 0.7%). In summary, in contrast with the differences in cortico-cortical connections that prompted a distinction between dorsorostral and ventrocaudal PGm (Passarelli et al. 2018), the site of origin of claustro-cortical connections was very similar throughout this area.

Area MIP

Area MIP was identified based on its myeloarchitecture and cortico-cortical connections, which were distinct from those of adjacent SPL areas. Like PGm, there were subtle differences in emphasis of connections between anterior and posterior injections, which hinted at a functional gradient (Bakola et al. 2017). Four tracer injections were placed within the borders of MIP (cases 3–6; see Table 1 and Fig. 1). Figure 5A shows the digital reconstruction of the claustrum of these cases.

In the two cases with injections in the posterior part of MIP (cases 3 and 4), labeled neurons were distributed across the full anteroposterior extent of the claustrum. However, in contrast with PGm injections, where claustral labeling was always quite uniform, following injections in posterior MIP, the majority of labeled neurons was concentrated in the posterior part of the claustrum (Fig. 5B, left) (63.1% and 72.5% in P-V sector and 19.3% and 7.9% in P-D sector, for cases 3 and 4, respectively). The bias toward connections originating in posterior claustrum was even more evident in the two cases with injections in anterior MIP (Fig. 5B, right) (88.7% and 71.9% in P-V sector and 5.1% and 26.3% in P-D sector, for cases 5 and 6, respectively).

Figure 6A shows the 3D reconstructions of claustrum of the four cases illustrated in Figure 5. Here, it is possible to better appreciate that, at anterior levels of the claustrum, the band of neurons that project to MIP tends to occupy a more dorsal location relative to that containing neurons projecting to PGm (compare Figs 4A and 6A). The histograms in Figure 6B show that labeling after MIP injections was mainly distributed in the posterior-ventral quadrant of claustrum; only posterior MIP injections revealed significant inputs from the anterior-dorsal quadrant.

Area V6Ad

Area V6Ad is adjacent to and functionally related to MIP. Altogether, these areas are components of the "parietal reach region" (Andersen et al. 1997, 2014; Bakola et al. 2017). Two injections (cases 1 and 2, see Table 1 and Fig. 1) were placed within the limits of area V6Ad. Both cases showed a similar pattern of label, but case 1, having relatively fewer labeled neurons, was not included in the quantitative analyses. Figure 7A shows a digital reconstruction of the claustrum in case 2. In general, the pattern of label strongly resembled that observed following injections in posterior MIP: labeled cells were concentrated in the posterior-ventral quadrant of the claustrum (86%), with a smaller but significant proportion (11%) occupying the anterior-dorsal quadrant. The similarity with posterior MIP is also evident in Figure 7B, where percentages of labeled cells at different coronal levels of the claustrum are shown. In contrast to the MIP cases, however, there were no projections to V6Ad from the posterior-dorsal claustrum.

Area 31

Area 31 is located on the mesial surface of the parietal lobe, immediately anterior to PGm, but is distinct from the latter by the increased emphasis on inputs from areas involved in somatomotor planning (Passarelli et al. 2018). After injection in area 31 (case 10), the pattern of label in the claustrum was in some ways intermediate between those found after the injections in PGm and posterior MIP: input neurons were observed along the full antero-posterior extent, with a bias toward posterior regions, but in this case largely avoiding the orbital sector of the claustrum (Fig. 7D, right; Fig. 7E).

Our quantitative analysis showed that the most strongly projecting region to area 31 was the posterior-ventral quadrant (63% of the labeled cells; Fig. 7E, right), with the anterior-dorsal and posterior-dorsal quadrants, respectively, containing 17% and 15% of the labeled cells. Label in the anterior-ventral quadrant was sparse, but somewhat greater in comparison to the injections in MIP and V6Ad (6%).

Area PEci

Area PEci is adjacent to area 31 but located on the posterior tip of the cingulate gyrus. Like area 31, PEci has been linked to higher order somatomotor function (Murray and Coulter 1981). An injection into PEci (case 9) resulted in claustral labeling which was similar to that observed after the injection in area 31, but seemed to extend further dorsally in the posterior part of the claustrum (Fig. 7D, left; Fig. 7E). This was confirmed in the quantitative analysis, which showed a majority of label in the posterior-dorsal quadrant (70%; Fig. 7E, right), with substantial proportions of labeled neurons in the posterior-ventral (14%) and the anterior-dorsal (14%) quadrants.

Area PEip

In a previous study (Gamberini et al. 2017), we described the claustral input to two areas located on the surface of the SPL (areas PE and PEc), which exhibit similar density of connections from areas that emphasize somatosensory function. The present experiments allowed us to extend this analysis to the sector of area PE embedded in the lateral bank of the intraparietal sulcus (area PEip; Bakola et al. 2017). An injection in area PEip (case 8) revealed afferents that were mainly confined in the posterior part of the claustrum (Fig. 8A, top; Fig. 8B, black columns). Quadrant analysis showed that the most strongly projecting region to area PEip was the posterior-dorsal quadrant (62% of the labeled cells; Fig. 8C, black columns), followed by the postero-ventral quadrant (22%). The anterior quadrants contributed fewer afferents (16% in total). As discussed below, this distribution was similar to that found following injection in PEci.

Area LIP

Finally, we compare the distribution of claustral afferents following SPL injections with the results of an injection in area LIP, which is an area of the inferior parietal lobule, more closely related to visuomotor function (Elston and Rosa 1998; Chen et al. 2016). This injection (case 7) revealed label along the

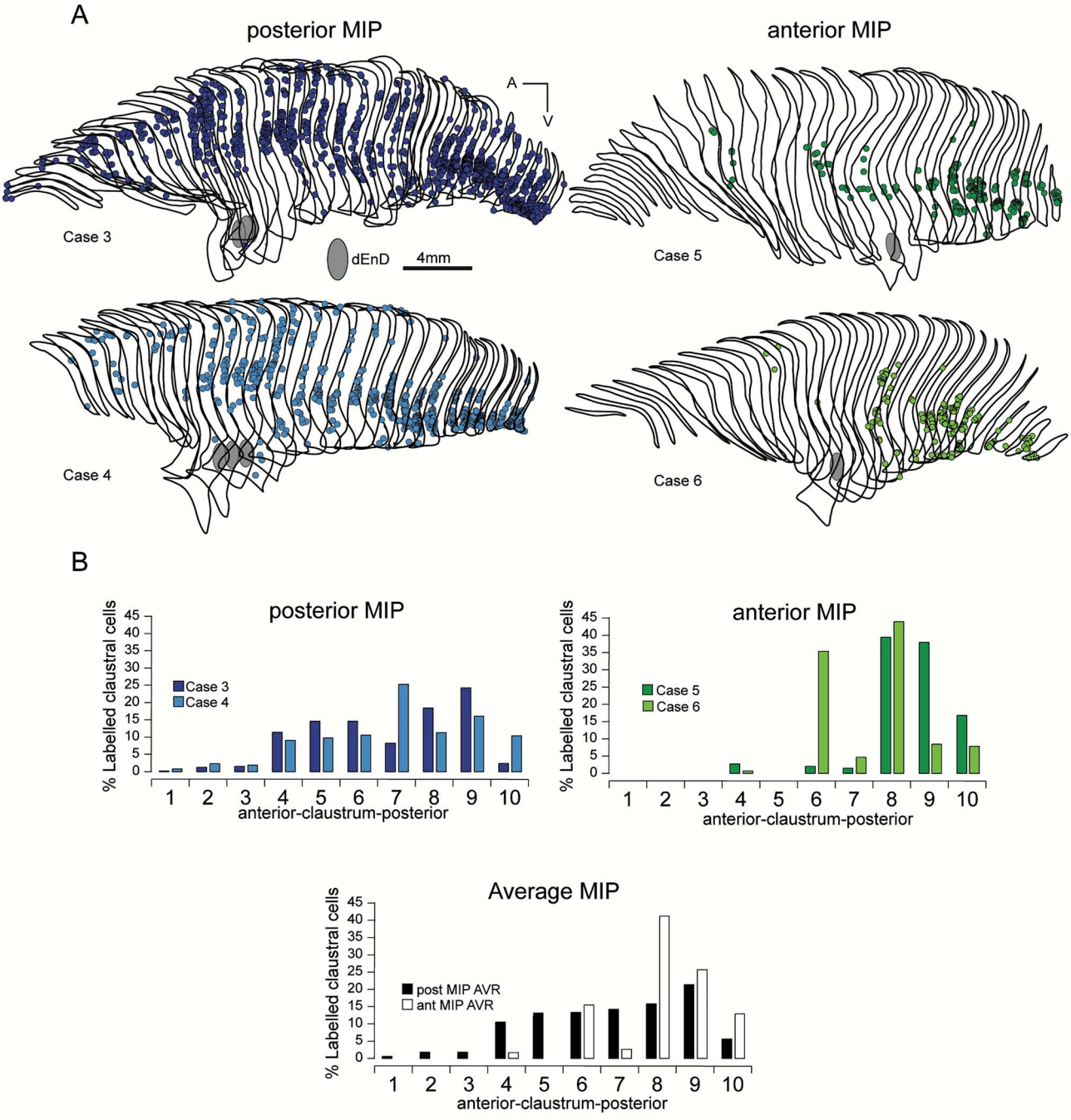

Figure 5. Claustral afferents to posterior and anterior portions of area MIP. (*A*) Outlines of the claustrum in MIP cases, sectioned in the coronal plane. Locations of single-labeled neurons are shown as colored circles. Scale bar = 4 mm. (*B*) Percentage of labeled cells in intervals corresponding to 10% of the claustrum along the rostro-caudal axis. Other details and abbreviations as in Figures 1 and 3.

full anteroposterior extent of claustrum. Similar to the PGm injections, labeled cells were located mainly in the ventral part of the claustrum, but in this case, they completely avoided the dorsal part of the structure at posterior levels (Fig. 8A, bottom). The labeling distribution according to quadrants (Fig. 8C, white columns) showed that the majority of labeled neurons was located in the posterior-ventral quadrant (48%), with substantial numbers also located in the anterior-dorsal (24%) and anterior-ventral (27%) quadrants.

Statistical Comparisons among the Different Injected Areas

We performed statistical evaluations of the similarity in the distribution of labeled cells across different injections (Fig. 9). We used two different approaches to explore possible segregation of claustral cells directly connected with the different medial posterior parietal areas: the anteroposterior level analysis and the quadrant analysis.

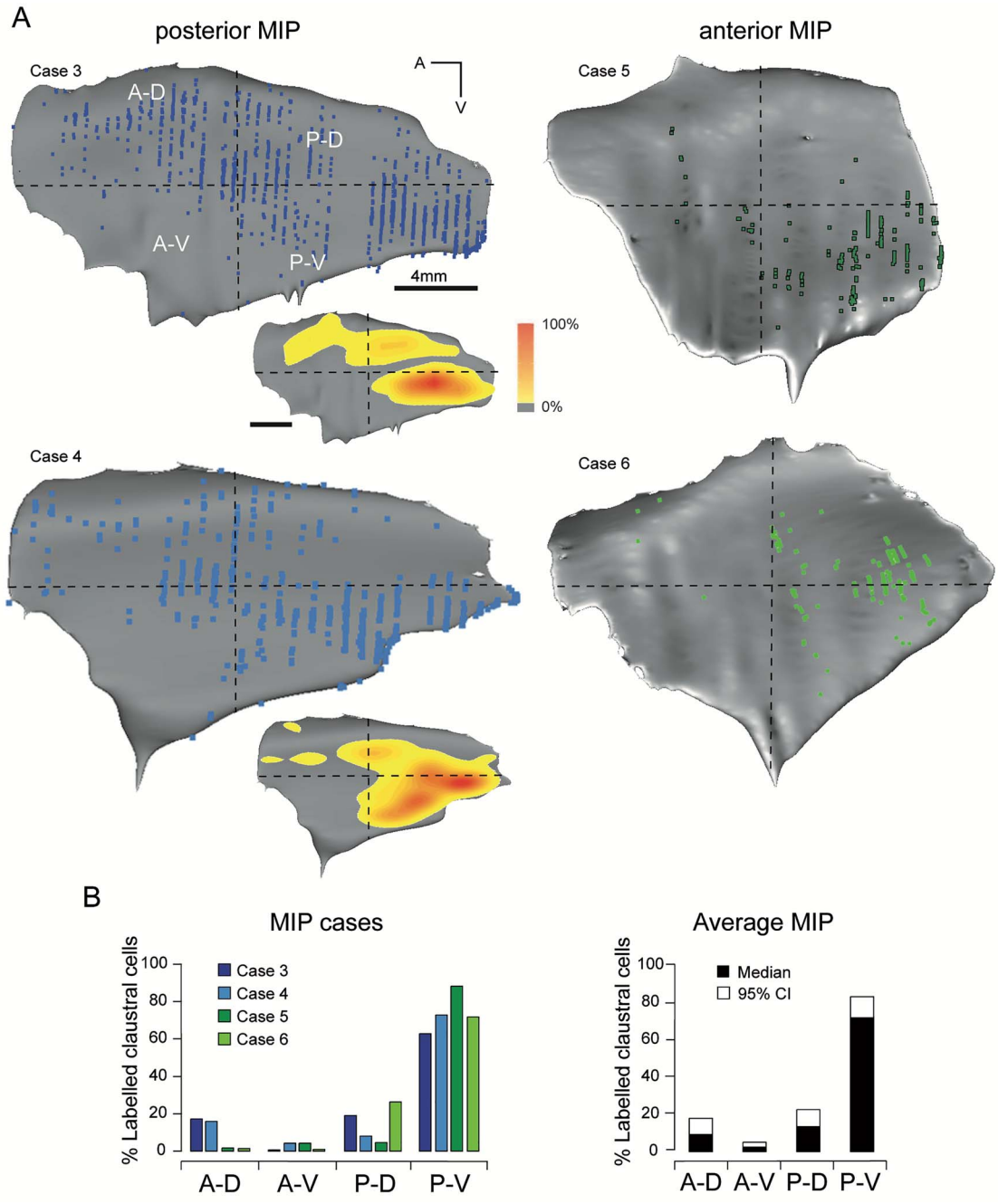

Figure 6. Claustral afferents to area MIP. (A) Medial views of 3D reconstructions of the claustrum of MIP cases shown in Figure 5, illustrating the distribution (single colored dots) and density (in color scale) of labeled cells of MIP cases. Density maps have been included only for posterior MIP cases, because anterior MIP cases had fewer labeled cells. Scale bar = 4 mm. (B) Percentage of labeled cells in the four quadrants of the claustrum after injections confined within the myeloarchitectonic limits of area MIP (Bakola et al. 2017). Other details and abbreviations as in Figures 1, 3, and 4.

Afferents to area PGm were homogeneously distributed within the claustrum, and there was no significant difference between the projections to dorsorostral and ventrocaudal PGm subdivisions, as shown by both the interval and the quadrant analyses ($W = 0.87$ in interval; $W = 1$ in quadrant). In contrast, the claustral afferents to area MIP showed a significant difference between injections in posterior and anterior parts of MIP, which is more evident in the analyses based on the quadrants ($W = 0.94$ in interval; $W = 0.70$ in quadrant), hinting at intra-areal variability of function.

Claustral afferents to area V6Ad showed a good level of similarity with those of MIP, in particular its posterior part, in both types of analyses ($W = 0.81$ in interval; $W = 0.90$ in quadrant). On the mesial surface of the hemisphere, by taking the interval approach, areas 31 and PEci showed a similar pattern of cell distribution ($W = 0.90$), but not in the quadrant approach ($W = 0.60$), where area 31 appeared more similar to MIP ($W = 1$ with MIPp) and PGm ($W = 0.70$). Finally, in the intraparietal sulcus, areas PEip and LIP showed an opposite pattern: PEip showed similarity with all areas of the SPL, except V6Ad, in the interval approach

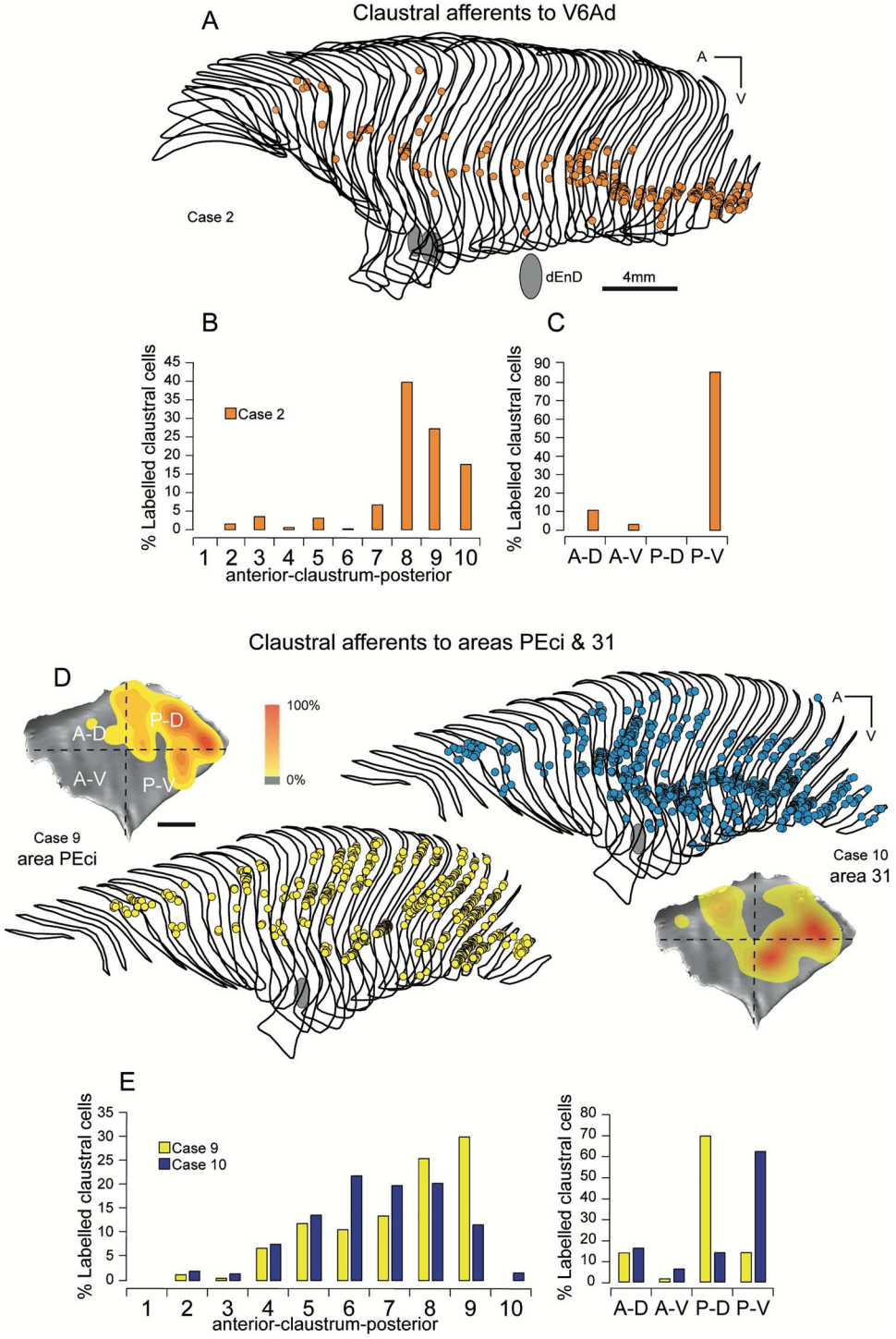

Figure 7. Claustral afferents to areas V6Ad, PEci and 31. (*A*) Outlines of the claustrum in V6Ad (case 2), sectioned in the coronal plane. Locations of single-labeled neurons are shown as orange circles. Scale bar = 4 mm. (*B*) Percentage of labeled cells in 10 anteroposterior intervals for the same case. (*C*) Percentage of labeled cells in the four quadrants of the claustrum after injection confined within the architectonic limits of area V6Ad (Luppino et al. 2005) in case 2. (*D*) Outlines of the claustrum and medial views of 3D reconstructions illustrating the density in cases with injections in areas PEci and 31, sectioned in the coronal plane. Locations of single-labeled neurons are shown as colored circles. Scale bar = 4 mm. (*E*) Left, Percentage of labeled cells in 10 intervals for PEci and area 31 cases. Right, Percentage of labeled cells in the four quadrants of the claustrum after injections confined within the cytoarchitectonic limits of areas PEci and 31. Other details and abbreviations as in Figures 1, 3, and 4.

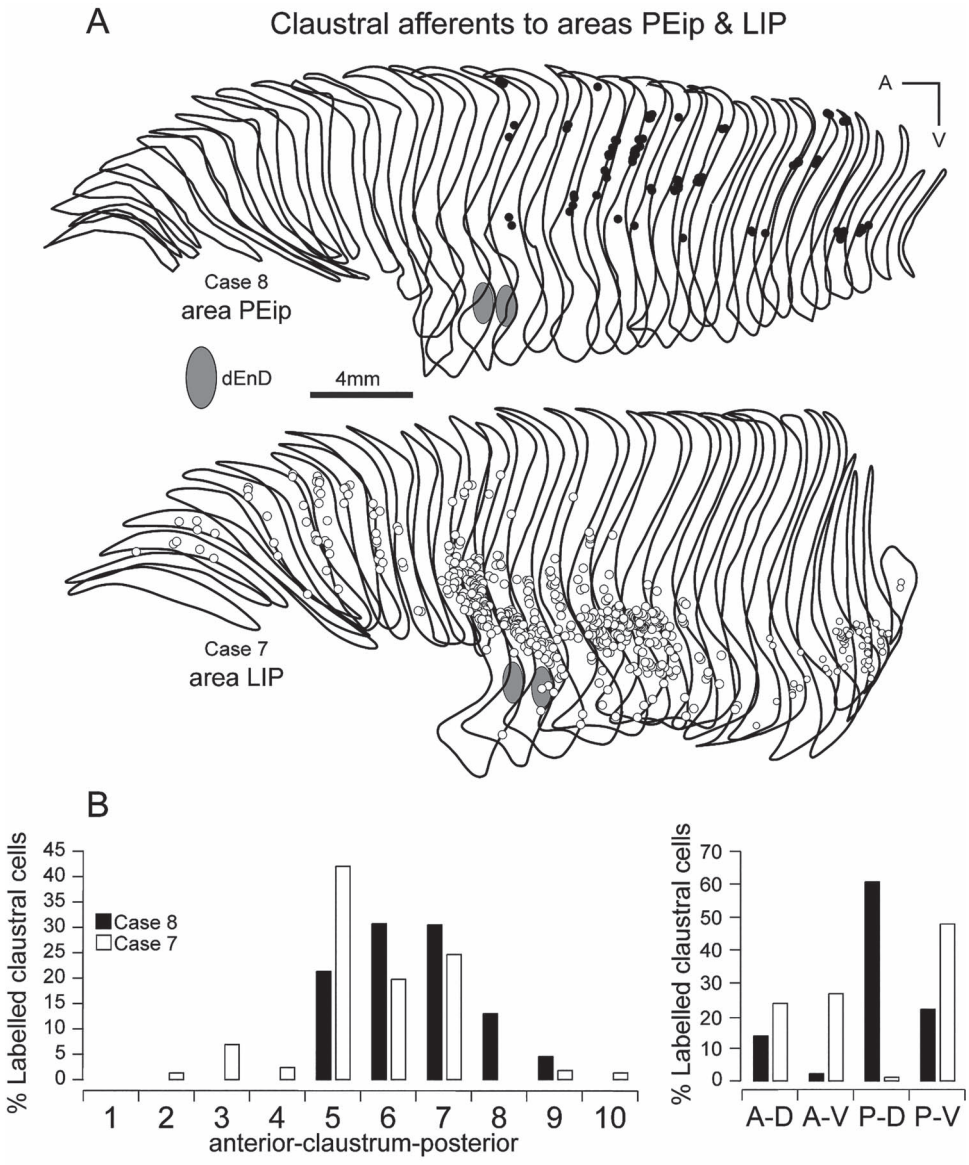

Figure 8. Claustral afferents to areas PEip and LIP. (*A*) Outlines of the claustrum in PEip and LIP cases, sectioned in the coronal plane. Locations of single-labeled neurons are shown as colored circles. Scale bar = 4 mm. (*B*) Percentage of labeled cells in 10 intervals for the area PEip and LIP cases. (*C*) Percentage of labeled cells in the four quadrants of the claustrum after injections confined within the myeloarchitectonic limits of areas PEip and LIP (Bakola et al. 2017). Other details and abbreviations as in Figures 1, 3, and 4.

(W = 0.64), while LIP did not. In the quadrant approach, PEip (like PEci) showed strong differences in the spatial distribution of labeled cells with the remaining areas.

Discussion

The aim of the present report was to describe the origins of claustral projections to cortical areas in the medial posterior parietal cortex. The present results, together with those of our previous study on claustral inputs to areas 2, PE, and PEc (Gamberini et al. 2017), show that each of the areas studied receives monosynaptic afferents from the claustrum. Moreover, although the origins of projections to each area were spread over large sectors of the claustrum, regional differences were detected using quantitative methods. As discussed in detail below, these results argue against simple models whereby adjacency between two areas in the cortex determine adjacency in their claustral origin of projections, or that the claustral projections are organized according to anatomical sectors of cortex they target (e.g., the occipital, parietal, temporal frontal, and limbic lobes). Instead, they indicate that subnetworks defined by commonality of function may be an important factor in defining claustrocortical topography.

Possible Limitations of the Study

Before discussing the implications of the present results, it is important to acknowledge some of the likely limitations of our study. Quantitative comparisons of results obtained by tracer injections can be difficult due to factors such as the effective

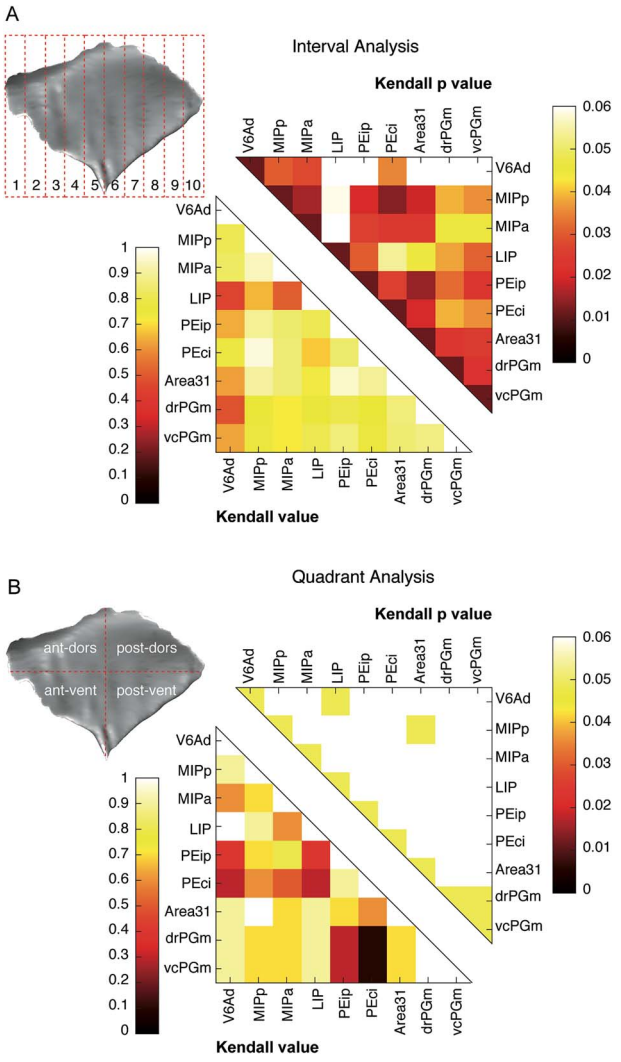

Figure 9. Statistical comparison of the similarity in the distribution of labeled cells among the different areas of medial posterior parietal cortex. Kendall rank correlation coefficient W measures the agreement between sets of ranks. Kendall coefficient W is 0 when there is complete disagreement in sets of ranks (black) and 1 when there is perfect agreement (white). Kendall *P*-value shows the statistical significance of the Kendall test: if $P < 0.05$ (toward black color), we reject the null hypothesis and so we can consider the tested areas similar. (*A*) Result of Kendall test (Kendall value and Kendall *P*-value) considering the labeled cell counts in 10 intervals. (*B*) Result of Kendall test (Kendall value and Kendall *P*-value) considering the labeled cell counts in the four quadrants.

spread of tracer in the tissue and the chemical characteristics of the different tracers. For example, larger injections in our sample tended to label larger numbers of neurons (Fig. 1B), and organometallic compounds such as DY and FB tended to label larger numbers of cells, compared with similar volumes of dextran-based tracers such as FR. Although the proportions of labeled versus unlabeled cells are expected to vary between cases based on these factors, the spatial distributions of the labeled cells in an afferent structure, including in particular the locations of the densest patches, are not known to be affected. Thus, our data are expected to faithfully reflect the topography of claustrocortical connections to the parietal lobe. In addition, although it may be difficult to precisely delineate the uptake zones, all injections included here were centered away from the borders of the areas, this removing a possible confound. Another possible limitation of our study is related to the use of different species of macaque. Yet, we found that the morphology of the claustrum was consistent across all cases, and the criteria used to identify parietal areas could be applied consistently, suggesting that the neural circuits studied in the present study do not vary substantially within this genus. Finally, some of the areas received a single injection of tracer. The consistency of the label location revealed in areas that received multiple injections suggests that there is a systematic relationship between locations of projection neurons in the claustrum and cortical area, but additional work may be needed to reveal the full extent of the complexity of the claustrocortical connectivity to the parietal lobe.

The claustrum is comprised of a relatively small number of neuron types (Kowiański et al. 1999; Smith, Alloway et al. 2019). In this study, all labeled cells were claustrocortical projection neurons (Kim et al. 2016), given that we used exclusively monosynaptic tracers. Some of the tracers employed tend to label only the cell nucleus (e.g., DY) or perikaryon (e.g., FB, CTB), which precludes finer analyses of soma size or morphology. Claustrum projection neurons are generally thought to be excitatory, with their cortical targets predominantly on inhibitory interneurons (reviewed in Jackson et al. 2020). However, this organization is best characterized in rodents, and although the basic organization in primates is similar, there is far less information available, suggesting that this is an area in need of further study.

Regional Segregation of Function in the Claustrum

The SPL areas we studied are all involved, in different ways, in the planning and controlling of reaching and grasping actions (Andersen et al. 1997; Ferraina et al. 1997; Galletti et al. 1997, 2003; Kalaska et al. 1997; Fattori et al. 2001, 2004, 2017; Andersen and Cui 2009). Indeed, the rare functional studies focused on the claustrum suggest that this structure is active in the context of arm movements (Shima et al. 1996; Gamberini et al. 2017), at least in the motor control of upper limbs during "hand-to-mouth" actions (Frontera and Stiehl 1963; Edelstein and Denaro 2004). Likewise, both area LIP and area PGm have been regarded as oculomotor fields, with the latter also having a putative role in eye-body coordination during self-motion and navigation (Andersen et al. 1990; Olson et al. 1996; Sato et al. 2006, 2010; Passarelli et al. 2018).

Previous studies from different laboratories have already emphasized the large overlap between the sectors of claustrum that project to different areas, with only a rough topography being evident. For example, it has been reported that frontal areas are mainly connected with the anterior part of the claustrum, parietal areas with posterior and dorsal parts, and occipital areas with posterior and ventral parts (Pearson et al. 1982; Maioli et al. 1983; Sherk 1986; Tanné-Gariépy et al. 2002; Baizer et al. 2014; Gattass et al. 2014; Gamberini et al. 2017; Bruni et al. 2018). Our results are in partial agreement with this view, in the sense that many of the parietal areas studied received most of their afferents from the posterior half of the claustrum. However, the exact distribution varied, with some areas (e.g., PGm, LIP) showing more substantial projections from the anterior and ventral sectors of the claustrum. Moreover, the neurons forming projections to most posterior parietal areas extended into the ventral sector of the posterior claustrum. Thus, our results, while compatible with those of earlier investigations of claustral input to the parietal lobe, provide a significant extension of the picture

they suggested, by providing a more nuanced view. Overall, our results are incompatible with a model based on simple spatial transformation, whereby adjacent sectors of cortex are predictably connected to adjacent sectors of the claustrum. Rather, they suggest a rather complex topology, which incorporates variability in the neuronal populations that project to different medial parietal areas.

The present results can be best related to the hypothesis of the existence of a functionally determined topography within the claustrum, a notion which has been previously hinted at by other authors (Gattass et al. 2014; Reser et al. 2017). For example, we know that the macaque posterior parietal cortex includes cortical areas dominated by somatic inputs, located anteriorly (PE, PEip, PEci, and PEc), as well as areas that have a documented role in visuomotor transformations (V6Ad, PGm, MIP, and LIP) (Elston and Rosa 1998; Bakola et al. 2017; Passarelli et al. 2018; Gamberini et al. 2020). All examined parietal areas received monosynaptic afferents from the posterior half of the claustrum. However, areas dominated by somatic processing (Fig. 10B) tended to receive relatively stronger inputs from the dorsal part of the claustrum, whereas areas involved in visuomotor cognition (PGm and LIP in particular) had relatively stronger inputs from the posterior ventral quadrant and generally stronger inputs from the anterior claustrum (Fig. 10C), even though they are distant from each other. Conversely, the claustral origins of PEip (somatically dominated) and of LIP (visually dominated) appeared to occupy largely distinct zones (Fig. 8), although whether this separation is complete will require studies using double labeling in the same animal.

These findings suggest that cortical subnetworks defined by commonality of function may be one of the key factors that explain claustrocortical connectivity, and add plausibility to the idea that the claustrum may have a role in coordination of activity across different resting state networks (e.g., Reser et al. 2014). Interestingly, according to this view, the pattern of origin of claustral projections to area 31 would suggest an as yet not fully recognized function involving visuomotor cognition, given the similarity with other visuomotor areas (Fig. 10C).

Cytoarchitectural characteristics provide a complementary framework to interpret these results. A recent review focused on the macaque SPL (Gamberini et al. 2020) proposed that Brodmann's area 5 is formed by somatically dominated functional subdivisions (PE, PEci, PEip), while area 7 primarily includes bimodal (somatosensory-visual) areas (PEc, V6A, PGm, MIP). By and large, the distribution of claustral cells projecting to the SPL described in the present study is compatible with the view that this neuroanatomical characteristic aligns with cytoarchitectural areas (Fig. 10). However, area PEc is an exception to this model, by virtue of its claustral input more closely resembling the pattern observed for subdivisions of area 5. Nonetheless, the predominance of somatosensory responses in this area, despite many bimodal neurons (Gamberini et al. 2018), suggests an alignment with the functional topography model discussed above. Cytoarchitectural characteristics are a predictor with connectivity patterns (Goulas et al. 2019), but different interpretations of cytoarchitectural borders can influence conclusions based on structure–function relationship models.

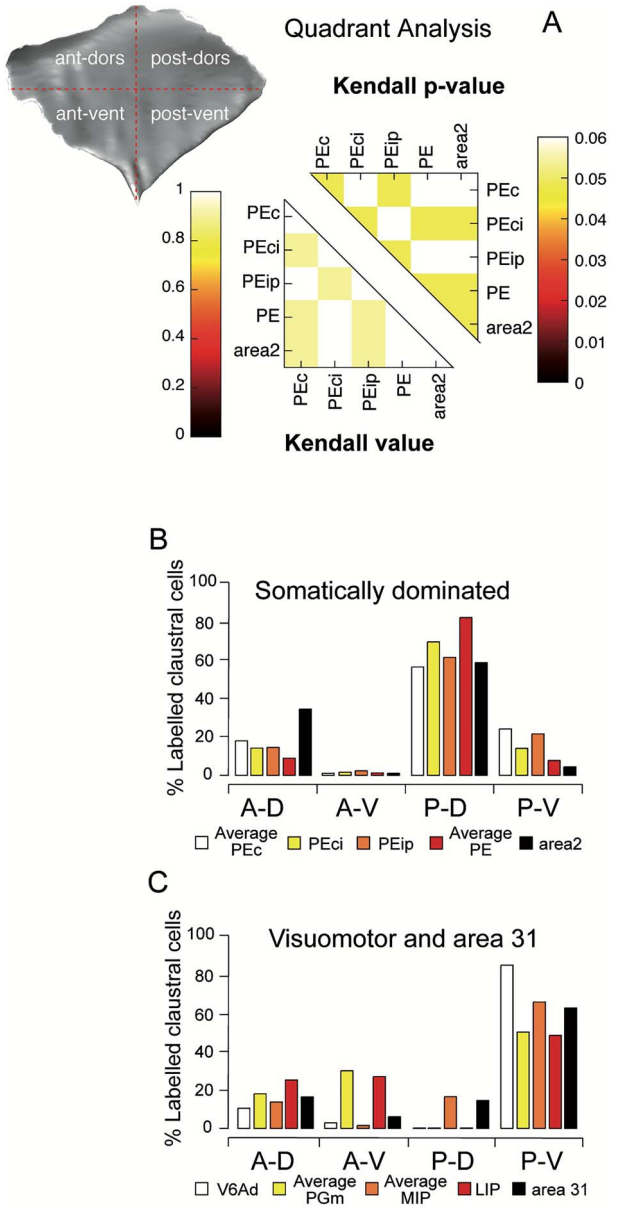

Figure 10. Patterns of claustral input to somatic and visuomotor areas. (A) Result of Kendall test (Kendall value and Kendall *P*-value) considering the labeled cell counts in the four quadrants, in somatically dominated areas. Areas PEci and PEip have been compared with results from Gamberini et al. (2017). (B) The pattern of connections of the somatically dominated areas includes PEc, PEci, PEip, PE, and area 2 (percentage of labeled cells in the four quadrants of the claustrum). (C) The pattern of connections of the visuomotor areas including V6Ad, PGm, MIP, and LIP (percentage of labeled cells in the four quadrants of the claustrum). Area 31 is included here given its similarity in claustral inputs with visuomotor areas.

Putative Integrative Functions of the Claustrocortical Network

In parallel with models based on regional segregation of function, it has been proposed that the claustrum is involved in the integration of signals from different sensory modalities to facilitate rapid shifts in attention, in line with environmental demands (Spector et al. 1975; Ettlinger and Wilson 1990; Edelstein and Denaro 2004; Remedios et al. 2014; Goll et al. 2015; Gamberini et al. 2017). These functional demands suggest roles for the widespread projections from claustrum to the dorsal posterior parietal cortex, as these complex behaviors require selective attention to the targets, feedback with respect

to the successful completion of the movement, and integration of specific sensory information with mnemonic processes (e.g., visual information may or may not be available). The variation in sensory information available during complex reaching and grasping movements would, in this context, lead to a variation in the cognitive load required to complete a given task. Variation in attention under differing levels of cognitive load and/or signal to noise ratio is consistent with a role for the claustrum in attention tasks with higher, but not lower, cognitive load (White et al. 2020).

Some studies in humans could help in understanding the possible functional role(s) of claustrum. It has been reported that the claustrum is involved in conscious behavior and cognition (Volz et al. 2010; Tian et al. 2011) and in the process of global perceptual integration (Baizer et al. 2014), with dysfunction possibly contributing to delusional states (Patru and Reser 2015). Lesion effects following traumatic brain injuries have been associated with "the duration, but not frequency, of loss of consciousness," and this suggests that the claustrum may have a role in regaining, but not maintaining, consciousness (Chau et al. 2015). Focal electrical stimulation concentrated in the posterior part of the claustrum caused sensory-motor effects but failed to induce the loss of consciousness (Bickel and Parvizi 2019). The sensory-motor effects evoked by the electrical stimulation of posterior claustrum are in line with the strong connections of this part of the claustrum with the posterior SPL as described in this study.

At the same time, anatomical changes linked to the evolutionary expansion of the cerebral cortex need to be taken into consideration when interpreting studies in macaques, including the possibility of human-specific connections (e.g., Ardesch et al. 2019). In particular, variation across species can be expected given the selective expansion of regions such as the precuneate cortex as a function of brain size (Chaplin et al. 2013). For example, it has been reported that the human precuneus is both disproportionately expanded and more variable across individuals in comparison with that of chimpanzees (Bruner et al. 2017). In the course of this expansion, the precuneus has segregated further into anterior and posterior components weighted toward processing of somatic and visual information, respectively (Bruner et al. 2019; Bruner and Pereira-Pedro 2020), reflecting an elaboration of the pattern found in the macaque (Passarelli et al. 2018). Although there is a strong possibility of significant changes in gradients of claustrum-cortical connectivity during human evolution, we currently lack the information about the functional organization of the claustrum in humans which would be necessary to evaluate this hypothesis.

In summary, the present results add to the evidence in the literature that the claustrum is in a position to coordinate activity between different cortical areas. Detailed anatomical studies, especially compared with functional studies of the same cortical regions, can inform on these issues. In particular, the characteristics of the projections to the medial posterior parietal cortex may inform future models of claustrum function in the context of volitional coordination of goal-directed behaviors.

Supplementary Material

Supplementary material is available at *Cerebral Cortex* online.

Funding

Australian Research Council (CE140100007, DE120102883, DP140101968); National Health and Medical Research Council (1020839, 1082144); European Union Grant (FP7-PEOPLE-2011-IOF 300452 to S.B.); H2020-MSCA-734227-PLATYPUS and Ministero dell'Università e della Ricerca (2017KZNZLN); Fondazione del Monte di Bologna e Ravenna and Fondazione Cassa di Risparmio di Bologna (Bando Internazionalizzazione), Italy.

Notes

We thank K.E. Richardson, M. Verdosci, and F. Campisi for technical assistance; L. Rinaldi and S. Bai for helping in the statistical analysis and for developing MatLab and Python scripts useful in the data analysis and representation; and Ms. Simran Bhopal for assistance with photography of histological sections. *Conflict of Interest*: The authors declare that they have no conflict of interest.

References

Andersen RA, Andersen KN, Hwang EJ, Hauschild M. 2014. Optic ataxia: from Balint's syndrome to the parietal reach region. *Neuron*. 81:967–983.

Andersen RA, Asanuma C, Essick G, Siegel RM. 1990. Corticocortical connections of anatomically and physiologically defined subdivisions within the inferior parietal lobule. *J Comp Neurol*. 296:65–113.

Andersen RA, Cui H. 2009. Intention, action planning, and decision making in parietal-frontal circuits. *Neuron*. 63:568–583.

Andersen RA, Snyder LH, Bradley DC, Xing J. 1997. Multimodal representation of space in the posterior parietal cortex and its use in planning movements. *Annu Rev Neurosci*. 20:303–330.

Atlan G, Terem A, Peretz-Rivlin N, Sehrawat K, Gonzales BJ, Pozner G, Tasaka G, Goll Y, Refaeli R, Zviran O, et al. 2018. The claustrum supports resilience to distraction. *Curr Biol*. 28:2752–2762.e7.

Ardesch DJ, Scholtens LH, Li L, Preuss TM, Rilling JK, van den Heuvel MP. 2019. Evolutionary expansion of connectivity between multimodal association areas in the human brain compared with chimpanzees. *Proc Natl Acad Sci U S A*. 116:7101–7106.

Baizer JS, Desimone R, Ungerleider LG. 1993. Comparison of subcortical connections of inferior temporal and posterior parietal cortex in monkeys. *Vis Neurosci*. 10:59–72.

Baizer JS, Sherwood CC, Noonan M, Hof PR. 2014. Comparative organization of the claustrum: what does structure tell us about function? *Front Syst Neurosci*. 8:117.

Bakola S, Passarelli L, Huynh T, Impieri D, Worthy KH, Fattori P, Galletti C, Burman KJ, Rosa MGP. 2017. Cortical afferents and myeloarchitecture distinguish the medial intraparietal area (MIP) from neighboring subdivisions of the macaque cortex. *eNeuro*. 4:ENEURO.0344–ENEU17.2017.

Bickel S, Parvizi J. 2019. Electrical stimulation of the human claustrum. *Epilepsy Behav*. 97:296–303.

Brodmann K. 1909. *Vergleichende Lokalisationslehre der Großhirnrinde in ihren Prinzipien dargestellt auf Grund des Zellenbaues*. Leipzig: Barth.

Brown SP, Mathur BN, Olsen SR, Luppi P-H, Bickford ME, Citri A. 2017. New breakthroughs in understanding the role of functional interactions between the neocortex and the claustrum. *J Neurosci*. 37:10877–10881.

Bruner E, Preuss T, Chen X, Rilling J. 2017. Evidence for expansion of the precuneus in human evolution. *Brain Struct Funct*. 222:1053–1060.

Bruner E, Esteve-Altava B, Rasskin-Gutman D. 2019. A network approach to brain form, cortical topology and human evolution. *Brain Struct Funct*. 224:2231–2245.

Bruner E, Pereira-Pedro S. 2020. A metric survey on the sagittal and coronal morphology of the precuneus in adult humans. *Brain Struct Funct*. 225:2747–2755.

Bruni S, Gerbella M, Bonini L, Borra E, Coudé G, Ferrari PF, Fogassi L, Maranesi M, Rodà F, Simone L, Serventi FU, Rozzi S. 2018. Cortical and subcortical connections of parietal and premotor nodes of the monkey hand mirror neuron network. *Brain Struct Funct*. 223:1713–1729.

Chaplin TA, Yu HH, Soares JG, Gattass R, Rosa MGP. 2013. A conserved pattern of differential expansion of cortical areas in simian primates. *J Neurosci*. 33:15120–15125.

Chau A, Salazar AM, Krueger F, Cristofori I, Grafman J. 2015. The effect of claustrum lesions on human consciousness and recovery of function. *Conscious Cogn*. 36: 256–264.

Chen M, Li B, Guang J, Wei L, Wu S, Liu Y, Zhang M. 2016. Two subdivisions of macaque LIP process visual-oculomotor information differently. *Proc Natl Acad Sci U S A*. 113:E6263–E6270.

Crick FC, Koch C. 2005. What is the function of the claustrum? *Philos Trans R Soc B Biol Sci*. 360:1271–1279.

Edelstein LR, Denaro FJ. 2004. The claustrum: a historical review of its anatomy, physiology, cytochemistry and functional significance. *Cell Mol Biol*. 50:675–702.

Elston GN, Rosa MGP. 1998. Complex dendritic fields of pyramidal cells in the frontal eye field of the macaque monkey: comparison with parietal areas 7a and LIP. *Neuroreport*. 9:127–131.

Ettlinger G, Wilson WA. 1990. Cross-modal performance: behavioural precesses, phylogenetic considerations and neural mechanisms. *Behav Brain Res*. 40:169–192.

Fattori P, Breveglieri R, Amoroso K, Galletti C. 2004. Evidence for both reaching and grasping activity in the medial parieto-occipital cortex of the macaque. *Eur J Neurosci*. 20: 2457–2466.

Fattori P, Breveglieri R, Bosco A, Gamberini M, Galletti C. 2017. Vision for prehension in the medial parietal cortex. *Cereb Cortex*. 27:1149–1163.

Fattori P, Breveglieri R, Raos V, Bosco A, Galletti C. 2012. Vision for action in the macaque medial posterior parietal cortex. *J Neurosci*. 32:3221–3234.

Fattori P, Gamberini M, Kutz DF, Galletti C. 2001. "Arm-reaching" neurons in the parietal area V6A of the macaque monkey. *Eur J Neurosci*. 13:2309–2313.

Ferraina S, Garasto MR, Battaglia-Mayer A, Ferraresi P, Johnson PB, Lacquaniti F, Caminiti R. 1997. Visual control of hand-reaching movement: activity in parietal area 7m. *Eur J Neurosci*. 9:1090–1095.

Frontera JG, Stiehl WL. 1963. Further results on stimulation of insula and claustrum in monkeys (*Macaca mulatta*). *Anat Rec*. 145:319–320.

Galletti C, Fattori P. 2018. The dorsal visual stream revisited: stable circuits or dynamic pathways? *Cortex*. 98:203–217.

Galletti C, Fattori P, Kutz DF, Battaglini PP. 1997. Arm movement-related neurons in the visual area V6A of the macaque superior parietal lobule. *Eur J Neurosci*. 9: 410–413.

Galletti C, Gamberini M, Kutz DF, Baldinotti I, Fattori P. 2005. The relationship between V6 and PO in macaque extrastriate cortex. *Eur J Neurosci*. 21:959–970.

Galletti C, Kutz DF, Gamberini M, Breveglieri R, Fattori P. 2003. Role of the medial parieto-occipital cortex in the control of reaching and grasping movements. *Exp Brain Res*. 153:158–170.

Gamberini M, Passarelli L, Bakola S, Impieri D, Fattori P, Rosa MGP, Galletti C. 2017. Claustral afferents of superior parietal areas PEc and PE in the macaque. *J Comp Neurol*. 525:1475–1488.

Gamberini M, Dal Bò G, Breveglieri R, Briganti S, Passarelli L, Fattori P, Galletti C. 2018. Sensory Properties of the Caudal Aspect of the Macaque Superior Parietal Lobule. *J Neurosci*. 223:1863–1879.

Gamberini M, Passarelli L, Fattori P, Galletti C. 2020. Structural connectivity and functional properties of the macaque superior parietal lobule. *Brain Struct Funct*. 225:1349–1367.

Gamberini M, Passarelli L, Fattori P, Zucchelli M, Bakola S, Luppino G, Galletti C. 2009. Cortical connections of the visuomotor parietooccipital area V6Ad of the macaque monkey. *J Comp Neurol*. 513:622–642.

Gattass R, Soares JGM, Desimone R, Ungerleider LG. 2014. Connectional subdivision of the claustrum: two visuotopic subdivisions in the macaque. *Front Syst Neurosci*. 8:63.

Goll Y, Atlan G, Citri A. 2015. Attention: the claustrum. *Trends Neurosci*. 38:486–495.

Goulas A, Majka P, Rosa MGP, Hilgetag CC. 2019. A blueprint of mammalian cortical connectomes. *PLoS Biol*. 17(3):e2005346.

Impieri D, Gamberini M, Passarelli L, Rosa MGP, Galletti C. 2018. Thalamo-cortical projections to the macaque superior parietal lobule areas PEc and PE. *J Comp Neurol*. 526:1041–1056.

Jackson J. 2018. Attention: noisy networks are tuned out by the claustrum. *Curr Biol*. 28:R937–R939.

Jackson J, Smith JB, Lee AK. 2020. The anatomy and physiology of claustrum-cortex interactions. *Ann Rev Neurosci*. 43: 231–247.

Kalaska JF. 1996. Parietal cortex area 5 and visuomotor behavior. *Can J Physiol Pharmacol*. 74:483–498.

Kalaska JF, Scott SH, Cisek P, Sergio LE. 1997. Cortical control of reaching movements. *Curr Opin Neurobiol*. 7:849–859.

Kim J, Matney CJ, Roth RH, Brown SP. 2016. Synaptic organization of the neuronal circuits of the claustrum. *J Neurosci*. 36:773–784.

Kowiański P, Dziewiatkowski J, Kowiańska J, Moryś J. 1999. Comparative anatomy of the claustrum in selected species: a morphometric analysis. *Brain Behav Evol*. 53: 44–54.

Legendre P. 2005. Species associations: the Kendall coefficient of concordance revisited. *J Agric Biol Environ Stat*. 10:226.

Luppino G, Ben Hamed S, Gamberini M, Matelli M, Galletti C. 2005. Occipital (V6) and parietal (V6A) areas in the anterior wall of the parieto-occipital sulcus of the macaque: a cytoarchitectonic study. *Eur J Neurosci*. 21:3056–3076.

Mai JK, Paxinos G. 2012. *The human nervous system*. 3rd ed. San Diego, Amsterdam: Academic Press/Elsevier.

Maioli MG, Squatrito S, Battaglini PP, Rossi R, Galletti C. 1983. Projections from the visual cortical region of the superior temporal sulcus to the striatum and claustrum in the macaque monkey. *Arch Ital Biol*. 121:259–266.

Mathur BN. 2014. The claustrum in review. *Front Syst Neurosci*. 8:48.

Milardi D, Bramanti P, Milazzo C, Finocchio G, Arrigo A, Santoro G, Trimarchi F, Quartarone A, Anastasi G, Gaeta M. 2015. Cortical and subcortical connections of the human claustrum revealed in vivo by constrained spherical deconvolution tractography. *Cereb Cortex*. 25:406–414.

Miyashita T, Nishimura-Akiyoshi S, Itohara S, Rockland KS. 2005. Strong expression of NETRIN-G2 in the monkey claustrum. *Neuroscience*. 136:487–496.

Morecraft RJ, Cipolloni PB, Stilwell-Morecraft KS, Gedney MT, Pandya DN. 2004. Cytoarchitecture and cortical connections of the posterior cingulate and adjacent somatosensory fields in the rhesus monkey. *J Comp Neurol*. 469:37–69.

Murray EA, Coulter JD. 1981. Supplementary sensory area. In: Woolsey CN, editor. *Cortical sensory organization: volume 1: multiple somatic areas*. Totowa (NJ): Humana Press, pp. 167–195.

Narikiyo K, Mizuguchi R, Ajima A, Shiozaki M, Hamanaka H, Johansen JP, Mori K, Yoshihara Y. 2020. The claustrum coordinates cortical slow-wave activity. *Nat Neurosci*. 23:741–753.

Olson CR, Musil SY, Goldberg ME. 1996. Single neurons in posterior cingulate cortex of behaving macaque: eye movement signals. *J Neurophysiol*. 76:3285–3300.

Pandya DN, Seltzer B. 1982. Intrinsic connections and architectonics of posterior parietal cortex in the rhesus monkey. *J Comp Neurol*. 204:196–210.

Passarelli L, Rosa MGP, Bakola S, Gamberini M, Worthy KH, Fattori P, Galletti C. 2018. Uniformity and diversity of cortical projections to precuneate areas in the macaque monkey: what defines area PGm? *Cereb Cortex*. 28:1700–1717.

Passarelli L, Rosa MGP, Gamberini M, Bakola S, Burman KJ, Fattori P, Galletti C. 2011. Cortical connections of area V6Av in the macaque: a visual-input node to the eye/hand coordination system. *J Neurosci*. 31:1790–1801.

Patru CM, Reser D. 2015. A new perspective on delusional states: evidence for claustrum involvement. *Front Psych*. 6:158.

Pearson RCA, Brodal P, Gatter KC, Powell TPS. 1982. The organization of the connections between the cortex and the claustrum in the monkey. *Brain Res*. 234:435–441.

Pham X, Wright DK, Atapour N, Chan JM-H, Watkins KJ, Worthy KH, Rosa M, Reichelt A, Reser DH. 2019. Internal subdivisions of the marmoset claustrum complex: identification by myeloarchitectural features and high field strength imaging. *Front Neuroanat*. 13:96.

Remedios R, Logothetis NK, Kayser C. 2014. A role of the claustrum in auditory scene analysis by reflecting sensory change. *Front Syst Neurosci*. 8:44.

Reser DH, Majka P, Snell S, Chan JMH, Watkins K, Worthy K, Quiroga MDM, Rosa MGP. 2017. Topography of claustrum and insula projections to medial prefrontal and anterior cingulate cortices of the common marmoset (*Callithrix jacchus*). *J Comp Neurol*. 525:1421–1441.

Reser DH, Richardson KE, Montibeller MO, Zhao S, Chan JMH, Soares JGM, Chaplin TA, Gattass R, Rosa MGP. 2014. Claustrum projections to prefrontal cortex in the capuchin monkey (*Cebus apella*). *Front Syst Neurosci*. 8:123.

Rosa MGP, Palmer SM, Gamberini M, Burman KJ, Yu H-H, Reser DH, Bourne JA, Tweedale R, Galletti C. 2009. Connections of the dorsomedial visual area: pathways for early integration of dorsal and ventral streams in extrastriate cortex. *J Neurosci*. 29:4548–4563.

Rosa MGP, Palmer SM, Gamberini M, Tweedale R, Piñon MC, Bourne JA. 2005. Resolving the organization of the new world monkey third visual complex: the dorsal extrastriate cortex of the marmoset (Callithrix jacchus). *J Comp Neurol*. 483:164–191.

Sato N, Sakata H, Tanaka YL, Taira M. 2006. Navigation-associated medial parietal neurons in monkeys. *Proc Natl Acad Sci U S A*. 103:17001–17006.

Sato N, Sakata H, Tanaka YL, Taira M. 2010. Context-dependent place-selective responses of the neurons in the medial parietal region of macaque monkeys. *Cereb Cortex*. 20:846–858.

Sherk H. 1986. The claustrum and the cerebral cortex. In: Jones EG, Peters A, editors. *Cerebral Cortex*. New York: Plenum, pp. 467–499.

Shima K, Hoshi E, Tanji J. 1996. Neuronal activity in the claustrum of the monkey during performance of multiple movements. *J Neurophysiol*. 76:2115–2119.

Siegel S. 1956. *Nonparametric statistics for the behavioral sciences*. New York: McGraw-Hill, p. 1956.

Smith JB, Alloway KD, Hof PR, Orman R, Reser DH, Watakabe A, Watson GDR. 2019. The relationship between the claustrum and endopiriform nucleus: a perspective towards consensus on cross-species homology. *J Comp Neurol*. 527:476–499.

Smith JB, Watson GDR, Liang Z, Liu Y, Zhang N, Alloway KD. 2019. A role for the claustrum in salience processing? *Front Neuroanat*. 13:64.

Smythies J, Edelstein L, Ramachandran V. 2012a. Hypotheses relating to the function of the claustrum. *Front Integr Neurosci*. 6:53.

Smythies J, Edelstein L, Ramachandran V. 2012b. The functional anatomy of the claustrum: the net that binds. *WebmedCentral Neurosci*. 3:WMC003182.

Smythies J, Edelstein L, Ramachandran V. 2014. Hypotheses relating to the function of the claustrum II: does the claustrum use frequency codes? *Front Integr Neurosci*. 8:7.

Spector I, Hassmannova J, Albe-Fessard D. 1975. Somatosensory properties of neurons in the cat's claustrum. In: Kornkuber HH, editor. *The somatosensory system*. Acton (MA): Science Publishing Group, pp. 135–144.

Tanné-Gariépy J, Boussaoud D, Rouiller EM. 2002. Projections of the claustrum to the primary motor, premotor, and prefrontal cortices in the macaque monkey. *J Comp Neurol*. 454: 140–157.

Team RC. 2014. *R: A language and environment for statistical computing*. Vienna, Austria [Internet]: R Foundation for Statistical Computing, 2015.

Tian F, Tu S, Qiu J, Lv JY, Wei DT, Su YH, Zhang QL. 2011. Neural correlates of mental preparation for successful insight problem solving. *Behav Brain Res*. 216:626–630.

Torgerson CM, Irimia A, Goh SYM, Van Horn JD. 2015. The DTI connectivity of the human claustrum. *Hum Brain Mapp*. 36:827–838.

Van Essen DC, Drury HA, Dickson J, Harwell J, Hanlon D, Anderson CH. 2001. An integrated software suite for surface-based analyses of cerebral cortex. *J Am Med Inform Assoc*. 8:443–459.

Volz KG, Schooler LJ, von Cramon DY. 2010. It just felt right: the neural correlates of the fluency heuristic. *Conscious Cogn*. 19:829–837.

White MG, Mu C, Qadir H, Madden MB, Zeng H, Mathur BN. 2020. The mouse claustrum is required for optimal behavioral performance under high cognitive demand. *Biol Psychiatry*. 88:719–726.

Wickham H. 2009. *Ggplot2: elegant graphics for data analysis*. New York: Springer.